IEEE Access
Multidisciplinary | Rapid Review | Open Access Journal

Received October 24, 2019, accepted November 9, 2019, date of publication November 19, 2019, date of current version December 4, 2019.

Digital Object Identifier 10.1109/ACCESS.2019.2954337

Expeditious Situational Awareness-Based Transmission Line Fault Classification and Prediction Using Synchronized Phasor Measurements

KUNJA BIHARI SWAIN[1], SATYA SOPAN MAHATO[2], AND MURTHY CHERUKURI[3], (Member, IEEE)

[1]Department of Electronics and Communication Engineering, Centurion University of Technology and Management, Paralakhemundi 761211, India
[2]Department of Electronics and Communication Engineering, National Institute of Science and Technology, Berhampur 761008, India
[3]Department of Electrical and Electronics Engineering, National Institute of Science and Technology, Berhampur 761008, India

Corresponding author: Murthy Cherukuri (chmurthy2007@gmail.com)

This work was supported by the Science and Engineering Research Board (SERB), Government of India, through the Early Career Research Award Category, under Grant ECR/2017/000812.

ABSTRACT The wide area situational awareness attempts at the expeditious detection of imminent system abnormalities and alerting system operators to take appropriate measures. Because the critical situation may arise in a system due to faults on transmission lines spanning over a long distance, phasor measurement units (PMUs) have become an indispensable measuring device to provide a dynamic view of such a wide area system. In this paper, the perception about a 200 km long transmission line has been achieved with the help of phasor measurements from PMU, which has the capability of reporting 200 phasors per second. The comprehension about the perceived event is accomplished by computing the deviations of current phasor magnitude as well as phase angles derived from synchronized phasor measurements using the phaselet algorithm. Based on the comprehension of the perceived event, a specific type of fault has been predicted using the Gaussian Naïve Bayes approach. In order to validate the proposed methodology, it has been implemented on a laboratory setup.

INDEX TERMS Phasor measurement units, power system protection, situational awareness, phaselet, Gaussian Naïve Bayes.

I. INTRODUCTION

The phasor measurement units (PMUs) have drastically enhanced the situational awareness (SA) of power system due to their ability to measure synchronized phasors of voltage and current of power system [1], [2] over a wide geographical area. SA has been a very effective aid for real-time monitoring and control of dynamic systems, such as the modern power system. The SA for the power system is defined as the perception about power system through measurements of different parameters, comprehension of the acquired data related to components for better situational awareness, and prediction of the state of power system based on comprehension of the acquired data [3], [4].

The associate editor coordinating the review of this manuscript and approving it for publication was Dusmanta Kumar Kumar Mohanta.

A. MOTIVATION

Transmission lines carry bulk power from generating units to the consumers traversing long distances. Thus, they are the key components of the power system. Since there is a separation of some hundreds of kilometers of distance from the sending end to the receiving end of the transmission lines, the synchronized phasor measurements (SPM) using PMUs have been an effective tool for real-time monitoring of both ends of the transmission line for wide area situational awareness (WASA). There has been an ongoing digital revolution pertaining to information and communication technologies (ICT). Consequently, there has been a paradigm shift regarding the perception of the power system from supervisory control and data acquisition (SCADA) to SPM. The data acquisition rate for SCADA is about 1-2 seconds, whereas the reporting rate of SPM is 50 phasors per second using full cycle discrete Fourier transform (FCDFT). The motivation of

this paper is to further enhance the perception for SA using Phaselet transform based synchronized phasor measurements with 4 times reporting rate, i.e., 200 phasors per second for 50Hz power system. Such a higher reporting rate of phasors improves the SA of transmission line for fault monitoring and control, as validated through real-time laboratory prototype model.

B. RELATED WORK

The modern power system has emerged as supreme engineering achievement comprising of the staggering number of interconnected components, spread over a large geographical area [5]. Thus, the synchronized phasor measurements have emerged as a commensurate wide area monitoring system (WAMS) using PMUs. The PMUs are the edifice of WAMS, which provide with the WASA.

Kamwa *et al.* has developed a smart WASA system for handling geomagnetic disturbance impacts on the grid through fast control and automated devices that utilize the phasor measurements. Wide area severity indices are derived from synchronized phasor measurements and fed to the corresponding predictors based on data mining models such as decision trees, random forests, neural networks and support vector machine to trade-off between accuracy and transparency [6], [7].

The first step for SA is perception. The high reporting rate, as well as the reliability of PMUs, directly contributes towards significant improvement regarding the perception for assessing WASA. Research findings reported in references [1]–[7] deal with the impact of PMUs on perception for evaluating SA. The effective perception of the transmission system for SA evaluation based on synchrophasor data has been utilized by many researchers for fault detection [8], [9]. These works have used the reporting rate of 50/60 phasors per second for the 50/60 Hz system using FCDFT. Though such real-time monitoring has improved the perception, there has been a continuous effort for improving reporting rates of phasors. The phaselet based synchrophasor computation uses one-fourth of a cycle of synchrophasor data, unlike FCDFT using data obtained from the full cycle. Thus, there has been an enhancement of perception leading to enhanced WASA.

The second step for SA is comprehension. The comprehension about the state of the transmission lines based on synchronized phasor measurements has been possible in real-time as reported by different researchers. Gopakumar *et al.* has proposed a novel adaptive transmission line fault identification and classification methodology based on the frequency domain analysis of the equivalent voltage and current phase angles estimated using PMU measurements at any one of the generator buses in the grid [8]. Using Park's transformation of measured three phase voltage and current phasors by the PMU at the generator bus, equivalent voltage and current phasor angles are estimated. FCDFT has been used to analyze the phase angles in real-time and also to compute the frequency spectrum coefficients. Thus, the comprehension of the perceived event taken on the transmission line was accomplished by computing the equivalent voltage and current phasor angles. Gopakumar *et al.* presented a methodology for detecting and identifying the location of a fault occurring anywhere in the network using the data obtained from PMUs [9]. The comprehension about the health of the transmission line has been achieved by considering the equivalent voltage phasor angle. Koteswar *et al.* has discussed the effect of static synchronous series compensator based subsynchronous resonance controller on the performance of distance relay. The problems associated with distance protection have been investigated using synchrophasor measurements based on the FCDT algorithm [10]. Asadi Majd *et al.* has proposed a K-NN based event detection and classification for distance protection by comparing each sample with its fifth sample by taking a half-cycle moving window [11]. Thus, they have adopted an efficient PMU data processing algorithm for better comprehension and improved situational awareness.

The third step for SA is the prediction based on the comprehension of the perceived event. The effective prediction of the fault on the transmission line for SA evaluation based on synchronized phasor measurements has been used by many researchers [12]–[14]. Fault prediction is accomplished by Rajaraman *et al.* using the zero sequence, negative sequence and positive sequence of currents [12]. The frequency coefficients of equivalent power factor angle variation and nominal voltage coefficients are used as inputs to the support vector machine (SVM) classifier for predicting the type of fault in reference [13]. A synchrophasor assisted protection scheme for the protection of a long transmission line compensated with the shunt FACTS device is presented in reference [14]. The proposed scheme has the ability to predict and discriminate internal and external faults using synchronized measurements of voltage and current phasors from both the ends of the transmission line. Thus, the prediction of fault on transmission lines using the data obtained from the PMUs leads to increased SA.

Thus, this paper attempts to adopt Phaselet based SA assessment for enhancing perception and comprehension about the health of the transmission line. The prediction based on Gaussian Naïve Bayes (GNB) also contributes significantly towards the enhancement of SA for the transmission line.

C. UNIQUE CONTRIBUTIONS

The unique contributions of the proposed work can be broadly segregated into four following aspects.

i. Expeditious perception for SA evaluation due to enhanced reporting rates (i.e., 4 times the conventional reporting rate) using Phaselet transform.
ii. Comprehension regarding transmission line SA using an efficient algorithm based on magnitude and phase angles of synchrophasor measurements of currents acquired at higher rates.
iii. Prediction of faults on a transmission line using Gaussian Naïve Bayes (GNB).

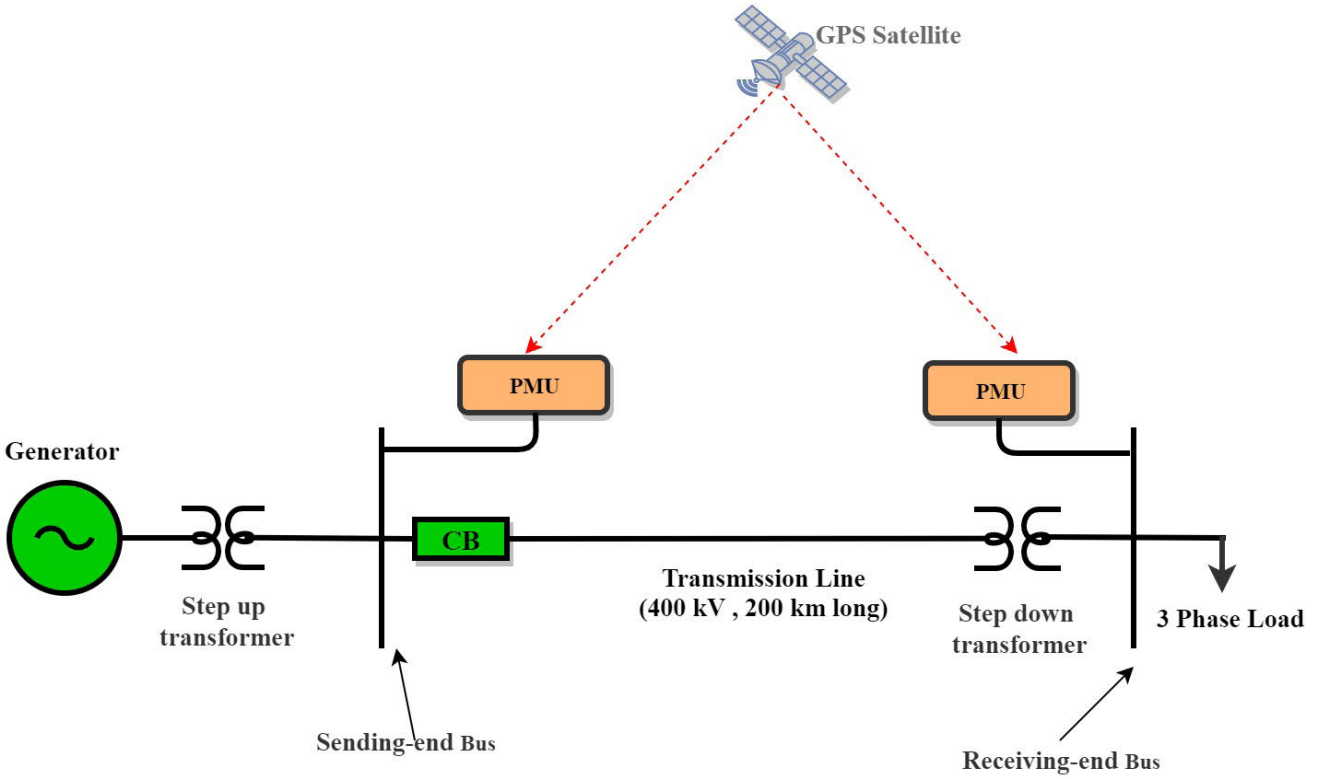

FIGURE 1. Single line diagram of a two-bus system.

iv. Validation of the proposed technique using real-time laboratory experimental setup for pragmatic applications.

D. ORGANISATION OF THE PAPER

The situational awareness assessment for the transmission line is discussed in section 2. In this section, the perception and comprehension about the state of the transmission line based on the SA perspective are elaborated. The prediction about the type of fault based on GNB is elaborated in section 3. Section 4 presents the case studies and result obtained from a real-time laboratory experimental setup. Conclusions are drawn in section 5.

II. SITUATIONAL AWARENESS ASSESSMENT FOR THE TRANSMISSION LINE

Synchronized phasor measurement (SPM) based real-time power grid surveillance offers sufficient SA for grid operators. The perception about the state of the transmission line during the normal condition, expeditious comprehension about the transition from normal to faulty state and the prediction of the specific type of fault using SPM are depicted in the following subsections. Fig. 1 represents a 400 kV, 200 km transmission line for a two-bus system. It consists of a generator, step-up transformer, sending end bus, one circuit breaker, a step-down transformer, receiving end bus and a three-phase load. Fig. 2 below gives an outline regarding the assessment of SA for the transmission line.

This section depicts the steps related to perception and comprehension for SA assessment so as to initiate a trip command to the relevant circuit breaker (CB) to isolate the faulty line at the earliest to minimize the hazard. Subsequent section deals with the prediction of fault.

A. PERCEPTION ABOUT THE STATE OF TRANSMISSION LINE

The perception about the state of the transmission line 400 kV, 200 km is based on the monitoring of the streaming phasors obtained from the PMUs located at two ends of the transmission line, as shown in Fig. 1. The prevailing algorithms for the computation of phasors by PMUs are based on FCDFT [1]. Such an algorithm employs a full cycle data window having a time period of 20ms for 50Hz, based on the following equation.

$$\hat{X}(k) = \frac{\sqrt{2}}{N}\sum_{n=0}^{N-1} x\,(n)\cos\left(\frac{2\pi n}{N}\right) - j\frac{\sqrt{2}}{N}\sum_{n=0}^{N-1} x\,(n)\sin\left(\frac{2\pi n}{N}\right) \quad (1)$$

where $\hat{X}(k)$ is the phasor for fundamental when k=1 as well as for harmonics for k $\geq$ 2; N is the total number of input samples per window (one cycle); n is the n^{th} sample and $x(n)$ is the input signal.

An expeditious phasor computation algorithm based phaselet is being employed for computation of SA in the

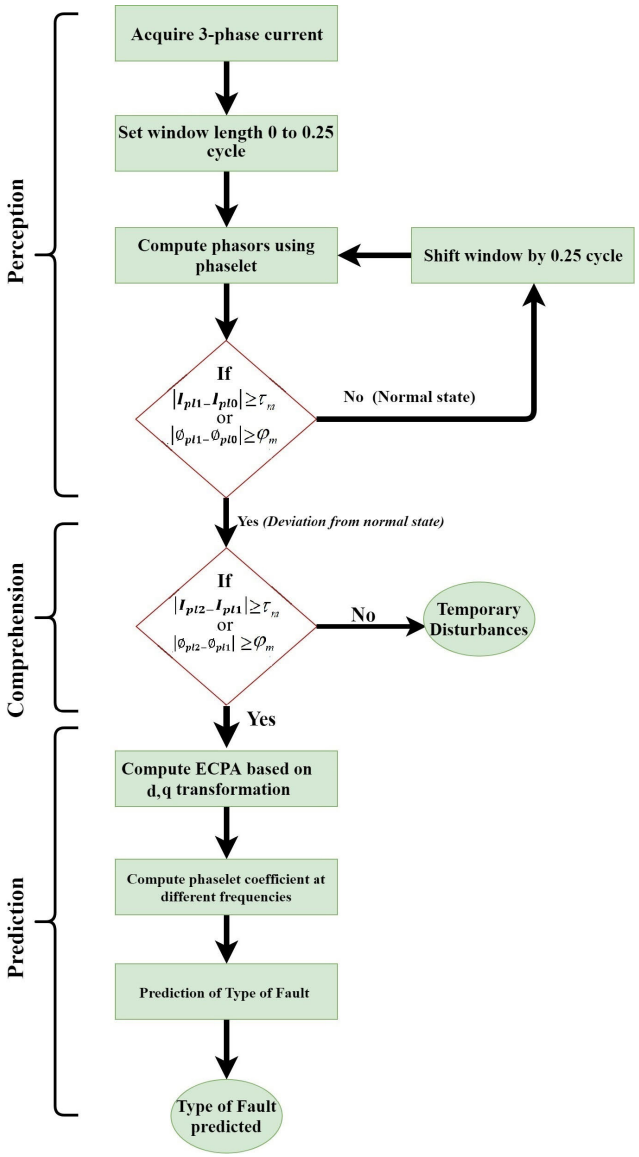

FIGURE 2. Flowchart for assessment of SA of transmission line.

proposed research work. Unlike the FCDFT based algorithm, the quarter of full-cycle phaselets (QFCP) utilizes a one-fourth cycle data window limited to 5ms [15], [16].

The computation of phasor based on phaselet transform is done based on equation (2), as given below,

$$\hat{X}_{pl}(k) = \frac{4\sqrt{2}}{N}\sum_{n=pl\times PL}^{pl\times PL+PL-1} x(n)\cos\left(\frac{2\pi n}{N}\right) - j\frac{4\sqrt{2}}{N}\sum_{n=pl\times PL}^{pl\times PL+PL-1} x(n)\sin\left(\frac{2\pi n}{N}\right) \quad (2)$$

where $\hat{X}_{pl}(k)$ is the phasor for fundamental when k=1 as well as for harmonics for k≥2; pl is phaselet index which varies from pl=0 to pl=3 for 4 phaselets; PL is the no of samples per phaselet (PL=50 for 200 samples/cycle);

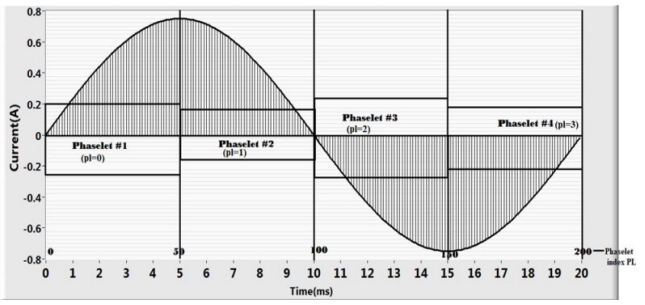

FIGURE 3. Phaselet based phasor computation.

n is n[th] sample; N is total number of samples per cycle and $x(n)$ is the input signal.

For example, considering sampling frequency 10kHz; Number of samples per cycle N=200; with a phaselet index PL=50 (50 samples per phaselet). The computations of phasors for each quarter cycle are illustrated using Fig. 3. Fig. 3 shows a 50 Hz signal sampled at 10^3 samples/sec for computation of four phaselets per cycle. Hence, there are 200 samples in a cycle. Each cycle (of 20 milliseconds duration) contains 200 samples and thus each phaselet contains 50 samples for a duration of 5 milliseconds. For the first phaselet, pl=0. So the beginning index of summation of equation (2) is n= pl×PL= 0×50=0 and the end index = pl×PL+PL−1= 0×50+50−1=49. Similarly, for the second phaselet, pl=1. So the beginning index is n=pl×PL=1×50 and the end index =pl×PL+PL−1= $1\times 50+50-1=99$. Likewise, for pl=2, the beginning index is 100 and the end index is 149 and for pl=3, the beginning index is 150 and the end index is 199. Thus, four phasors for fundamental frequency are obtained for one cycle during normal operation when harmonics are negligible. The magnitude and phase angle of the first phasor is represented by $|I_{pl0}|$ and $|\varphi_{pl0}|$, based on the initial 50 samples. Similarly, the second phasor magnitude $|I_{pl1}|$ and phase angle $|\varphi_{pl1}|$ is computed based on the second phaselet. If the deviation of $|I_{pl1}|$ from $|I_{pl0}|$ and $|\varphi_{pl1}|$ from $|\varphi_{pl0}|$ increases beyond the threshold values τ_m and φ_m respectively, then the perception about the transition from the normal state is perceived expeditiously within a time-span of a quarter of a cycle, as shown in Fig. 2. Since 4 phaselets $(I_{pl0}, I_{pl1}, I_{pl2}, I_{pl3})$ are being used for every cycle, expeditious perception is possible by capturing the changes in every quarter of cycle by each phaselet. Such perception is captured using a situational awareness visualization tool (SAVT), where the visual monitoring indicator changes from green (normal state) to yellow (fault state) color along with an alarm, as shown in Fig. 4. The specific type of fault is identified by the red color indicator.

B. COMPREHENSION ABOUT FAULT OCCURRENCE

After the perception of transition from the normal state based on streaming phasors computed using a quarter of cycle data for the phaselets I_{pl1} and I_{pl2}, the comprehension about the occurrence of the fault ascertained by comparing with another phaselet, namely I_{pl3} computed using half-cycle

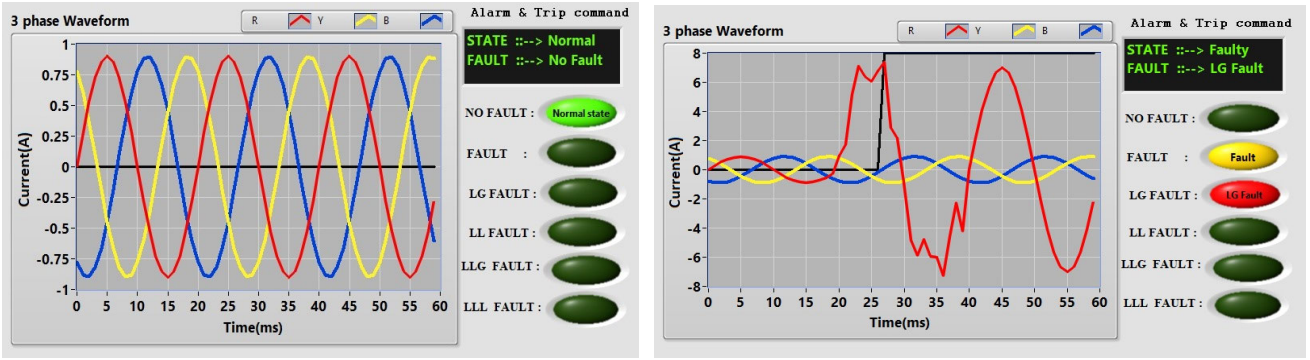

(a) (b)

FIGURE 4. Situational awareness visualization tool for perception of (a) Normal state, (b) Faulty state.

window (first quarter cycle as well as subsequent quarter cycle). If the deviations $|I_{pl3} - I_{pl2}|$ and $|\varphi_{pl3} - \varphi_{pl2}|$ are greater than threshold values τ_m and φ_m respectively, then conclusive comprehension about the occurrence of a fault is achieved. The SAVT indicates the comprehension about the occurrence of fault through the blinking of a red indicator as shown in Fig. 5. Thus the trip signal is initiated to open the circuit breaker at sending end of the transmission line, as shown in Fig. 1. The subsequent section deals with a prediction about the type of fault.

III. PREDICTION OF FAULT USING GNB

The GNB classifier maps the feature vector $\psi_{pl}(k)[\psi_{pl}(k = 0), \psi_{pl}(k = 1), \psi_{pl}(k = 2), \psi_{pl}(k = 3), \psi_{pl}(k = 4)]$ obtained from equivalent current phase angles (ECPA) of d.c component $\psi_{pl}(k = 0)$, fundamental $\psi_{pl}(k = 1)$, as well as harmonics of phase currents computed using phaselet coefficients with class level as shown in Fig. 2 for the purpose of training.

A Naïve Bayes is a simple model that is based on the probability evaluated from the training data set. This training data set comprises of ECPA coefficients both during normal as well as during different faults. GNB is an extended Naïve Bayes model suitable for real-time streaming data [17]–[19], as described in this section.

The ECPA is calculated using the direct and quadrature axis current components, namely $I_d(n)$ and $I_q(n)$ obtained from fundamental current phasors, as given in the equations (3a) and (3b), as shown at the bottom of this page [20].

$x_R(n), x_Y(n)$ and $x_B(n)$ are the values of currents of nth samples for phase R, Y and B respectively; and N is the number of samples per cycle.

ECPA is calculated using equation (4) and the Phaselet coefficients of the ECPA for d.c., fundamental and up to 4th harmonics are calculated using equation 5(a)-5(e) [8].

$$ECPA(\phi_{ei}(n)) = \tan^{-1}\left(\frac{I_q(n)}{I_d(n)}\right) \tag{4}$$

where $\phi_{ei}(n)$ is the ECPA for nth component. The component for n=0 denotes d.c., n=1 denotes fundamental and n =2, 3, 4 represents 2nd, 3rd and 4th harmonic values respectively for current phasors.

Phaselet coefficient of ECPA for d.c. component is as follows

$$\psi_{pl}(k) = \psi_{pl}(0) = \left(\frac{4\sqrt{2}}{N}\right) \sum_{n=pl.PL}^{pl.PL+PL-1} \phi_{ei}(n) \tag{5a}$$

Phaselet coefficient of ECPA for fundamental frequency

$$\psi_{pl}(k) = \psi_{pl}(1) = \left(\frac{4\sqrt{2}}{N}\right) \sum_{n=pl.PL}^{pl.PL+PL-1} \phi_{ei}(n).e^{-\left(\frac{2\pi n}{N}\right)} \tag{5b}$$

Similarly, the phaselet coefficients of ECPA for second, third and fourth harmonics are computed using the following equations (5c), (5d) and (5e).

$$\psi_{pl}(k) = \psi_{pl}(2) = \left(\frac{4\sqrt{2}}{N}\right) \sum_{n=pl.PL}^{pl.PL+PL-1} \phi_{ei}(n).e^{-\left(\frac{4\pi n}{N}\right)} \tag{5c}$$

$$\psi_{pl}(k) = \psi_{pl}(3) = \left(\frac{4\sqrt{2}}{N}\right) \sum_{n=pl.PL}^{pl.PL+PL-1} \phi_{ei}(n).e^{-\left(\frac{6\pi n}{N}\right)} \tag{5d}$$

$$\psi_{pl}(k) = \psi_{pl}(4) = \left(\frac{4\sqrt{2}}{N}\right) \sum_{n=pl.PL}^{pl.PL+PL-1} \phi_{ei}(n).e^{-\left(\frac{8\pi n}{N}\right)} \tag{5e}$$

$$I_d(n) = \frac{2}{3}\left[x_R(n).\sin\left(\frac{2\pi n}{N}\right) + x_Y(n).\sin\left(\frac{2\pi n}{N} - \frac{2\pi}{3}\right) + x_B(n).\sin\left(\frac{2\pi n}{N} + \frac{2\pi}{3}\right)\right] \tag{3a}$$

$$I_q(n) = \frac{2}{3}\left[x_R(n).\cos\left(\frac{2\pi n}{N}\right) + x_Y(n).\cos\left(\frac{2\pi n}{N} - \frac{2\pi}{3}\right) + x_B(n).\cos\left(\frac{2\pi n}{N} + \frac{2\pi}{3}\right)\right] \tag{3b}$$

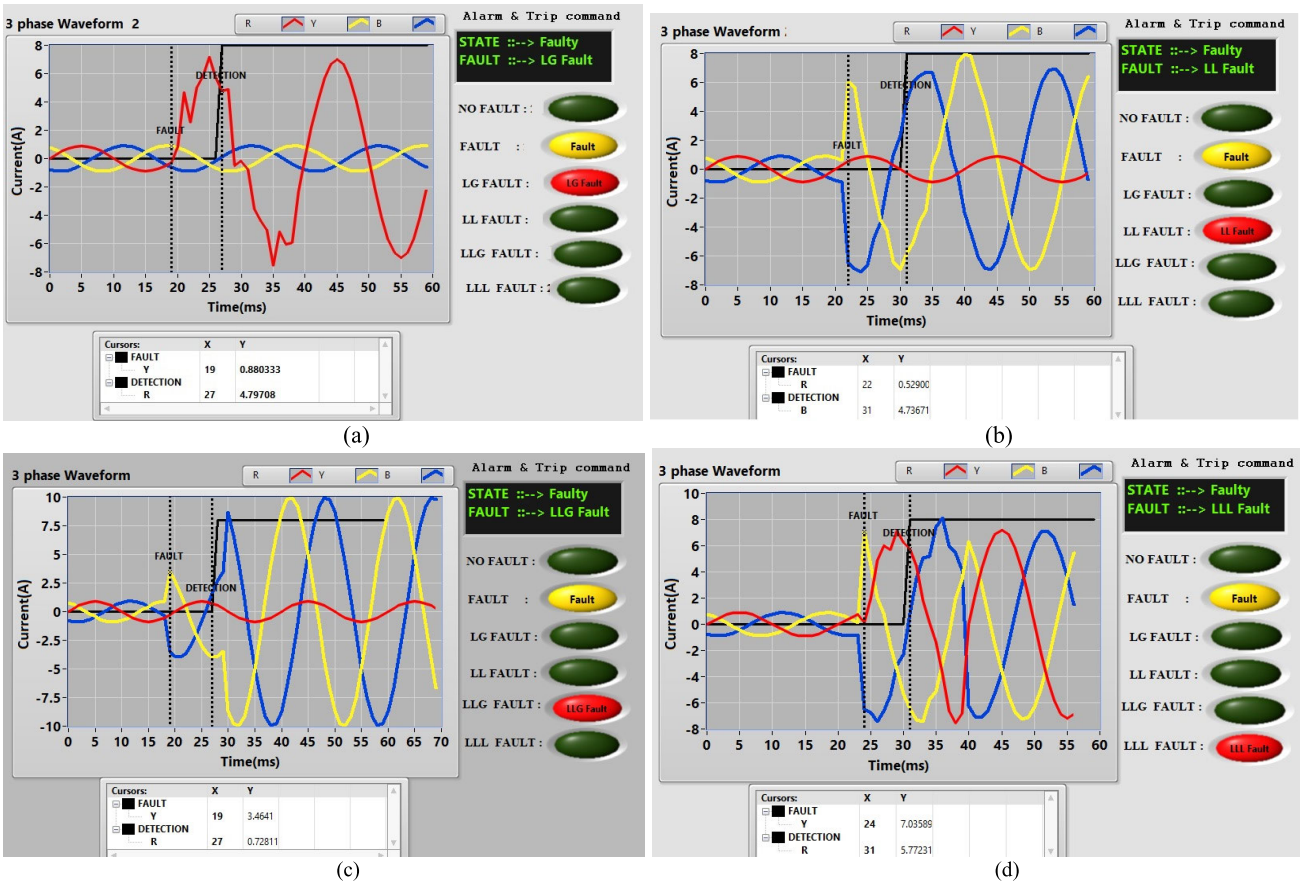

FIGURE 5. Situational awareness visualization tool for comprehension of (a) LG fault condition (b) LL fault condition (c) LLG fault condition (d) LLL fault condition.

The feature vector comprising of Phaselet coefficients $\psi_{pl}(k)$ contains attributes pertaining to normal state and 4 faulty states. The normal class cn belongs to the normal state of the transmission line. The possible faulty states are a line-ground fault (LG), line- line fault (LL), line-line-ground fault (LLG) and line-line-line fault (LLL). The classes for the faulty class represented as cn, cf1, cf2, cf3 and cf4. Thus, the class level vector Y$\in$ $(cn, cf1, cf2, cf3, cf4)$ contains 5 classes. Then the data set $\psi_{pl}(k)$ is segmented into each of 5 classes, viz. cn for the normal state, cf1 for LG fault, cf2 for LL fault, cf3 for LLG and cf4 for LLL fault respectively. Each feature vector C_i comprises of $\psi_{pl}(k)$ values for k=0, 1, 2, 3 for each phaselet. For example, for the first Phaselet (pl=0), the feature vector is $\psi_{pl}(k) = [\psi_0(0), \psi_0(1), \psi_0(2), \psi_0(3), \psi_0(4)]$. For a feature class cn, the $\psi_{pl}(k)$ are values obtained for the normal state. Similarly, feature classes $(cf1, cf2, cf3, cf4)$ comprise of feature data obtained during corresponding faults.

GNB uses two significant measures such as model construction and prediction to predict the type of fault as shown in Fig. 6. The model construction comprises of information table consisting of the mean (μ) and standard deviation (σ) of every attribute is calculated using equation (6), as shown at the bottom of the next page, and equation (7) viz. $\psi_{pl}(0)$, $\psi_{pl}(1)$, $\psi_{pl}(2)$, $\psi_{pl}(3)$ and $\psi_{pl}(4)$ for the training data set with a known fault class. Then the class probability of each class is calculated using equation (8). In the prediction stage, the probability distribution function (pdf) is calculated for each attribute of online test data using equation (9). Then the conditional probability is calculated for each class using equation (10). Finally, the fault is predicted by considering the class having the highest conditional probability.The mean for the normal state, LG fault, LL fault, LLG fault, and LLL is calculated as follows using equations (6a)-(6e). Similarly, the variance in normal state, LG fault, LL fault, LLG fault and LLL fault are calculated using equation (7a) -(7e).

$$\sigma^2\left[cn(k)\right] = \left[\psi_{pl,z}(k) - \mu\left[cn(k)\right]\right]^2 \tag{7a}$$

$$\sigma^2\left[cf1(k)\right] = \left[\psi_{pl,z}(k) - \mu\left[cf1(k)\right]\right]^2 \tag{7b}$$

$$\sigma^2\left[cf2(k)\right] = \left[\psi_{pl,z}(k) - \mu\left[cf2(k)\right]\right]^2 \tag{7c}$$

$$\sigma^2\left[cf3(k)\right] = \left[\psi_{pl,z}(k) - \mu\left[cf3(k)\right]\right]^2 \tag{7d}$$

$$\sigma^2\left[cf4(k)\right] = \left[\psi_{pl,z}(k) - \mu\left[cf4(k)\right]\right]^2 \tag{7e}$$

where $\psi_{pl,z}(k)$ denotes the phaselet coefficient of p^{th} phaselet, z^{th} sample; k =0 denotes the dc components; k=1 denotes fundamental component; k=2,3,4 denotes the second, third and fourth harmonics; z=1,2,3,4……Z.

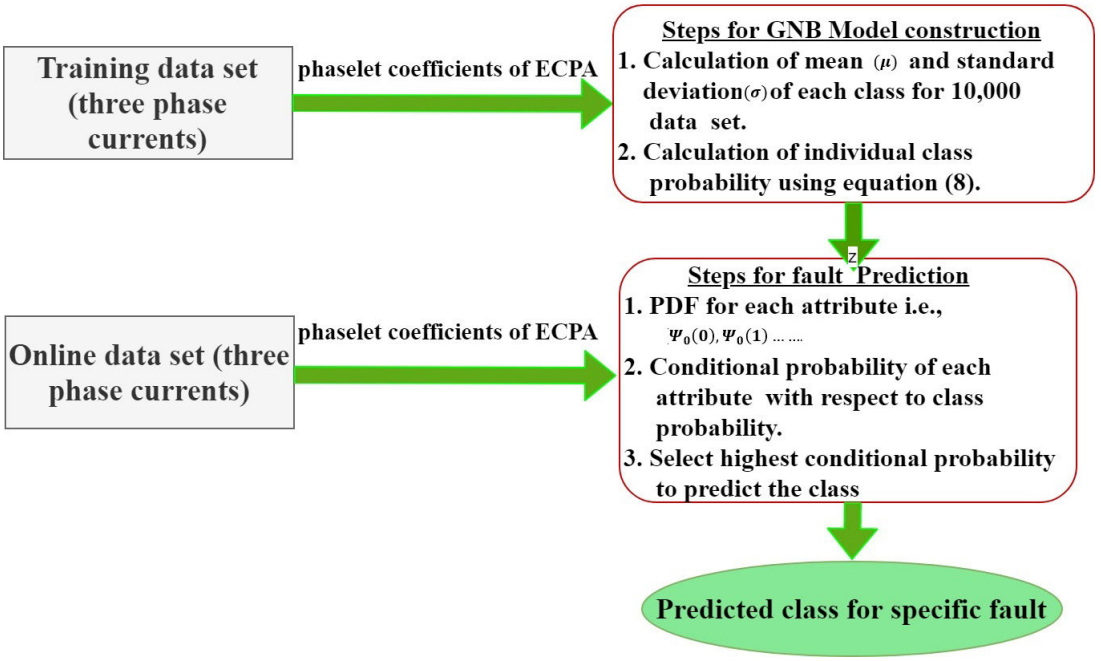

FIGURE 6. Prediction of the fault using GNB.

The class probability of class cn as shown in equation (8a) is defined as follows

$$P_{cn} = \frac{\text{Number of elements for class cn}}{\text{Total no of elements for all classes}} \tag{8a}$$

Similarly, the class probability for class cf1, class cf2, class cf3 and class cf4 are given in equation (8b) to equation (8e).

$$P_{cf1} = \frac{\text{Number of elements for class cf1}}{\text{Total no of elements for all classes}} \tag{8b}$$

$$P_{cf2} = \frac{\text{Number of element for class cf2}}{\text{Total no of elements for all classes}} \tag{8c}$$

$$P_{cf3} = \frac{\text{Number of elements for class cf3}}{\text{Total no of elements for all classes}} \tag{8d}$$

$$P_{cf4} = \frac{\text{Number of elements for class cf4}}{\text{Total no of elements for all classes}} \tag{8e}$$

The probability density function (PDF) is given in equation (9). The probability density function for the normal state is

$$\mu\,[cn(k)] = \frac{\psi_{0,1}(k)+\psi_{1,1}(k)+\psi_{2,1}(k)+\psi_{3,1}(k)+\psi_{0,2}(k)+\psi_{1,2}(k)+\psi_{2,2}(k)+\psi_{3,2}(k)+\ldots..+\psi_{0,z}(k)+\psi_{1,z}(k)+\psi_{2,z}(k)+\psi_{3,z}(k)}{Z\times 4} \tag{6a}$$

$$\mu\,[cf1(k)] = \frac{\psi_{0,1}(k)+\psi_{1,1}(k)+\psi_{2,1}(k)+\psi_{3,1}(k)+\psi_{0,2}(k)+\psi_{1,2}(k)+\psi_{2,2}(k)+\psi_{3,2}(k)+\ldots..+\psi_{0,z}(k)+\psi_{1,z}(k)+\psi_{2,z}(k)+\psi_{3,z}(k)}{Z\times 4} \tag{6b}$$

$$\mu\,[cf2(k)] = \frac{\psi_{0,1}(k)+\psi_{1,1}(k)+\psi_{2,1}(k)+\psi_{3,1}(k)+\psi_{0,2}(k)+\psi_{1,2}(k)+\psi_{2,2}(k)+\psi_{3,2}(k)+\ldots..+\psi_{0,z}(k)+\psi_{1,z}(k)+\psi_{2,z}(k)+\psi_{3,z}(k)}{Z\times 4} \tag{6c}$$

$$\mu\,[cf3(k)] = \frac{\psi_{0,1}(k)+\psi_{1,1}(k)+\psi_{2,1}(k)+\psi_{3,1}(k)+\psi_{0,2}(k)+\psi_{1,2}(k)+\psi_{2,2}(k)+\psi_{3,2}(k)+\ldots..+\psi_{0,z}(k)+\psi_{1,z}(k)+\psi_{2,z}(k)+\psi_{3,z}(k)}{Z\times 4} \tag{6d}$$

$$\mu\,[cf4(k)] = \frac{\psi_{0,1}(k)+\psi_{1,1}(k)+\psi_{2,1}(k)+\psi_{3,1}(k)+\psi_{0,2}(k)+\psi_{1,2}(k)+\psi_{2,2}(k)+\psi_{3,2}(k)+\ldots..+\psi_{0,z}(k)+\psi_{1,z}(k)+\psi_{2,z}(k)+\psi_{3,z}(k)}{Z\times 4} \tag{6e}$$

calculated using equation 9(a).

$$P_{df}\left(\psi_{pl}(k),\mu\left[cn(k)\right],\sigma\left[cn(k)\right]\right)=\frac{1}{\sigma\left[cn(k)\right]\sqrt{2\pi}}\times e^{-\left(\frac{(\psi_{pl}(k)-\mu[cn(k)])^2}{2\sigma[cn(k)]^2}\right)} \quad (9a)$$

Similarly for LG fault (cf1), LL Fault (cf2), LLG fault (cf3) and LLL fault (cf4), the PDFs are calculated using equations (9b)-(9e) respectively.

$$P_{df}\left(\psi_{pl}(k),\mu\left[cf1(k)\right],\sigma\left[cf1(k)\right]\right)=\frac{1}{\sigma\left[cf1(k)\right]\sqrt{2\pi}}\times e^{-\left(\frac{(\psi_{pl}(k)-\mu[cf1(k)])^2}{2\sigma[cf1(k)]^2}\right)} \quad (9b)$$

$$P_{df}\left(\psi_{pl}(k),\mu\left[cf2(k)\right],\sigma\left[cf2(k)\right]\right)=\frac{1}{\sigma\left[cf2(k)\right]\sqrt{2\pi}}\times e^{-\left(\frac{(\psi_{pl}(k)-\mu[cf2(k)])^2}{2\sigma[cf2(k)]^2}\right)} \quad (9c)$$

$$P_{df}\left(\psi_{pl}(k),\mu\left[cf3(k)\right],\sigma\left[cf3(k)\right]\right)=\frac{1}{\sigma\left[cf3(k)\right]\sqrt{2\pi}}\times e^{-\left(\frac{(\psi_{pl}(k)-\mu[cf3(k)])^2}{2\sigma[cf3(k)]^2}\right)} \quad (9d)$$

$$P_{df}\left(\psi_{pl}(k),\mu\left[cf4(k)\right],\sigma\left[cf4(k)\right]\right)=\frac{1}{\sigma\left[cf4(k)\right]\sqrt{2\pi}}\times e^{-\left(\frac{(\psi_{pl}(k)-\mu[cf4(k)])^2}{2\sigma[cf4(k)]^2}\right)} \quad (9e)$$

The conditional probability for class cn is found using equation (10a) as follows

$$\begin{aligned}P_{con,cn}&=P\left(P_{df}(\psi_{pl}(0),\mu\left[cn(0)\right],\sigma\left[cn(0)\right])\right)\\&\times P\left(P_{df}(\psi_{pl}(1),\mu\left[cn(1)\right],\sigma\left[cn(1)\right])\right)\\&\times P\left(P_{df}(\psi_{pl}(2),\mu\left[cn(2)\right],\sigma\left[cn(2)\right])\right)\\&\times P\left(P_{df}(\psi_{pl}(3),\mu\left[cn(3)\right],\sigma\left[cn(3)\right])\right)\\&\times P\left(P_{df}(\psi_{pl}(4),\mu\left[cn(4)\right],\sigma\left[cn(4)\right])\right)\end{aligned} \quad (10a)$$

Similarly, the conditional probability for class1, class2, class3 and class4 is found using equation (10b)-(10e)

$$\begin{aligned}P_{con,cf1}&=P\left(P_{df}(\psi_{pl}(0),\mu\left[cf1(0)\right],\sigma\left[cf1(0)\right])\right)\\&\times P\left(P_{df}(\psi_{pl}(1),\mu\left[cf1(1)\right],\sigma\left[cf1(1)\right])\right)\\&\times P\left(P_{df}(\psi_{pl}(2),\mu\left[cf1(2)\right],\sigma\left[cf1(2)\right])\right)\\&\times P\left(P_{df}(\psi_{pl}(3),\mu\left[cf1(3)\right],\sigma\left[cf1(3)\right])\right)\\&\times P\left(P_{df}(\psi_{pl}(4),\mu\left[cf1(4)\right],\sigma\left[cf1(4)\right])\right)\end{aligned} \quad (10b)$$

$$\begin{aligned}P_{con,cf2}&=P\left(P_{df}(\psi_{pl}(0),\mu\left[cf2(0)\right],\sigma\left[cf2(0)\right])\right)\\&\times P\left(P_{df}(\psi_{pl}(1),\mu\left[cf2(1)\right],\sigma\left[cf2(1)\right])\right)\\&\times P\left(P_{df}(\psi_{pl}(2),\mu\left[cf2(2)\right],\sigma\left[cf2(2)\right])\right)\\&\times P\left(P_{df}(\psi_{pl}(3),\mu\left[cf2(3)\right],\sigma\left[cf2(3)\right])\right)\\&\times P\left(P_{df}(\psi_{pl}(4),\mu\left[cf2(4)\right],\sigma\left[cf2(4)\right])\right)\end{aligned} \quad (10c)$$

$$\begin{aligned}P_{con,cf3}&=P\left(P_{df}(\psi_{pl}(0),\mu\left[cf3(0)\right],\sigma\left[cf3(0)\right])\right)\\&\times P\left(P_{df}(\psi_{pl}(1),\mu\left[cf3(1)\right],\sigma\left[cf3(1)\right])\right)\\&\times P\left(P_{df}(\psi_{pl}(2),\mu\left[cf3(2)\right],\sigma\left[cf3(2)\right])\right)\\&\times P\left(P_{df}(\psi_{pl}(3),\mu\left[cf3(3)\right],\sigma\left[cf3(3)\right])\right)\\&\times P\left(P_{df}(\psi_{pl}(4),\mu\left[cf3(4)\right],\sigma\left[cf3(4)\right])\right)\end{aligned} \quad (10d)$$

$$\begin{aligned}P_{con,cf4}&=P\left(P_{df}(\psi_{pl}(0),\mu\left[cf4(0)\right],\sigma\left[cf4(0)\right])\right)\\&\times P\left(P_{df}(\psi_{pl}(1),\mu\left[cf4(1)\right],\sigma\left[cf4(1)\right])\right)\\&\times P\left(P_{df}(\psi_{pl}(2),\mu\left[cf4(2)\right],\sigma\left[cf4(2)\right])\right)\\&\times P\left(P_{df}(\psi_{pl}(3),\mu\left[cf4(3)\right],\sigma\left[cf4(3)\right])\right)\\&\times P\left(P_{df}(\psi_{pl}(4),\mu\left[cf4(4)\right],\sigma\left[cf4(4)\right])\right)\end{aligned} \quad (10e)$$

where $P_{con,cn}$, $P_{con,cf1}$, $P_{con,cf2}$, $P_{con,cf3}$ and $P_{con,cf4}$ are the conditional probability with respect to class cn, class cf1, class cf2, class cf3 and class cf4 respectively; P is the probability with respect to a particular class.

IV. CASE STUDIES AND RESULTS

The proposed methodology has been implemented on an artificial transmission line to validate it in real-time. The block diagram of the experimental setup is shown in Fig. 7 and laboratory experimental setup is shown in Fig. 8. The experimental set up comprises of an equivalent per unit source, an isolation transformer, a three-phase autotransformer, a PMU interfaced with Dell Workstation, a 4-pole contactor, a 400 kV, 200 km transmission line and a three-phase star connected load. The line parameters are scaled-down by keeping the same per unit value of the experimental setup and the practical transmission line. The 440V, 3-phase AC supply has been considered as a generator. For safety reasons, a 440V/110V isolation transformer is placed after the generator. For performing the experiment with the variable voltage 110V/(0-110V), an autotransformer is connected after the isolation transformer. For isolating the transmission line in case of transmission line fault, a 4-pole contactor is provided after the autotransformer, which acts as a circuit breaker. It operates immediately after receiving the trip signal to isolate the transmission line. The circuit breaker is connected at the sending end of the transmission line. The transmission line consists of 4-π sections, each equivalent to 50 km, cascaded together to form a 200 km transmission line. The resistance, inductance and capacitance of each π section are 0.2Ω, 8.4mH and 2.0μ F respectively, which corresponds to 400 kV twin moose line. Each section is provided with tap-points to apply the fault using a fault block and taking the measurements. The fault block consists of push-button switches, which can create different short circuit (considering zero fault impedance) faults among the lines and ground. The current measurements of the transmission line are taken at the beginning of the first section (i.e., at 0km, sending end) and different types of faults are applied at 200 km (i.e., receiving end) of the transmission line. At the receiving end of the transmission line, a three-phase balanced resistive load of 1KΩ, 300V, 1.2 A and a three-phase 230V, 200W balanced lamp load has been used to carry out the experiment.

PMU comprises of data acquisition system consisting of a cRIO-9066 controller along with a NI-9246, NI-9242, a

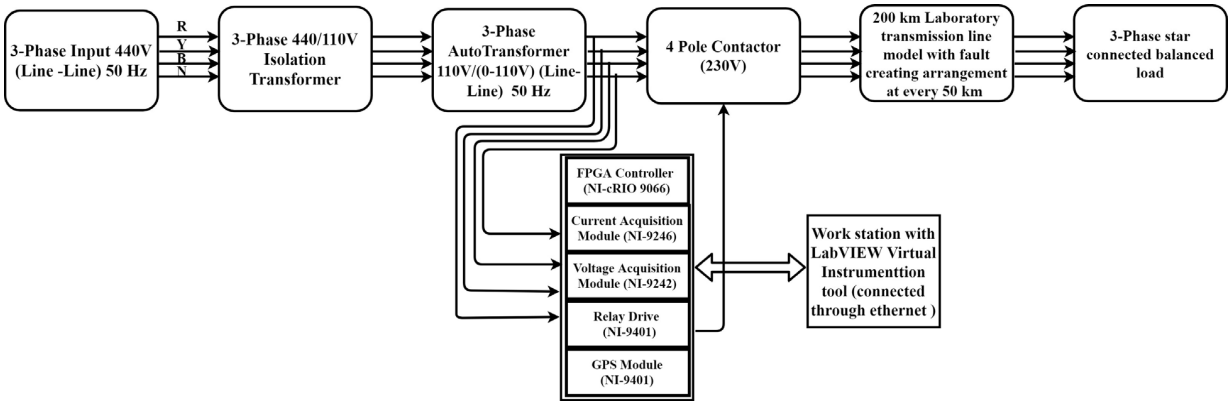

FIGURE 7. Block diagram of an experimental setup.

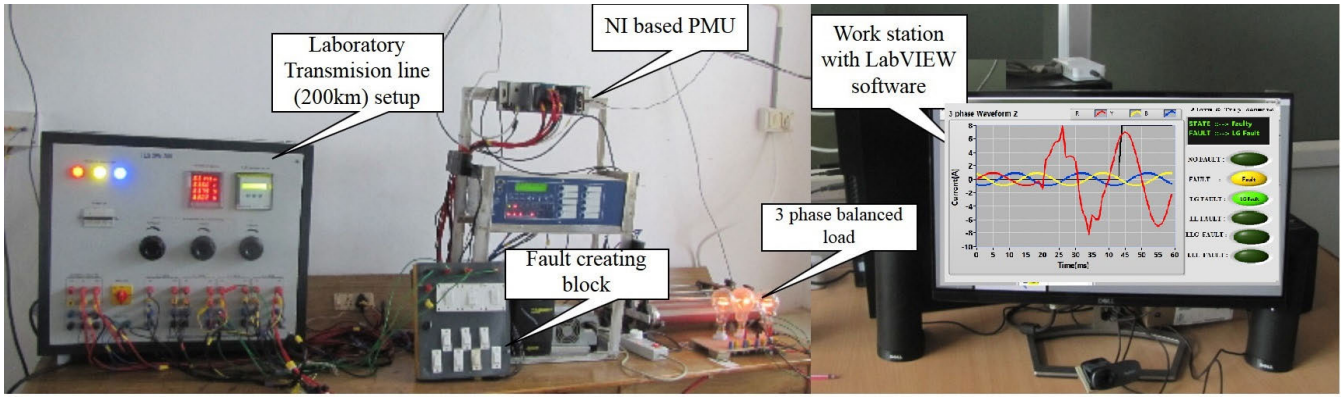

FIGURE 8. Laboratory experimental set up for transmission line with PMUs for synchronized phasor measurements.

TABLE 1. Phaselet based perception and comprehension of transmission line fault.

Fault Type		Instant of Fault (ms)	Instant of Detection (ms)	Time taken to detect (ms)
LG Fault	RG	20.00	27.00	7.00
	YG	23.45	31.15	7.70
	BG	24.80	32.30	7.50
LL Fault	RY	22.27	31.00	8.73
	YB	22.26	31.00	8.74
	BR	21.80	29.60	7.80
LLG Fault	RYG	22.27	31.00	8.73
	YBG	19.44	27.00	7.56
	BRG	21.80	29.80	8.00
LLL Fault	RYB	24.78	31.00	6.22

NI-9467 C Series GPS Synchronization Module and NI-9401 C series digital input-output module.

I. CompactRIO (NI cRIO-9066): It is an embedded real-time controller with reconfigurable FPGA for C Series Modules with 8 slots, build with 667 MHz Dual-Core CPU, 256 MegaByte DRAM and 512 MegaByte storage. In this setup, cRIO-9066 holds the C series modules, one in each slot. cRIO acts as an intermediate between Dell Workstation which runs LabVIEW to perform required computations in real-time and C series modules [21].

II. NI-9246: It is a 24-bit, 20 Ampere (rms), 30-Ampere peak-to-peak, three-phase AC current input module which is used as a current transformer (CT) for sensing three-phase AC current from the transmission line with a single NI-9246 module. It can sample the analog current at a rate of 50,000 samples per second per channel which can provide the sampling rate up to 50 kHz. In the present work, the sampling rate is 10 kHz [22].

III. NI-9242: It is a three-phase AC voltage input module of 250 Volt (rms) Line to neutral, 400 Volt (rms) Line-Line, 24 bit, three-channel voltage input module.

TABLE 2. Information table.

Normal (no-fault) condition (cn)				
For k=0 (d.c)	$P(\psi_0(0), Y = cn)$	$P(\psi_1(0), Y = cn)$	$P(\psi_2(0), Y = cn)$	$P(\psi_3(0), Y = cn)$
Mean	0.0227913	0.0227500	0.022754	0.02278
Standard deviation	0.000703	0.000789	0.000750	0.000719
For k =1 (Fundamental component)	$P(\psi_0(1), Y = cn)$	$P(\psi_1(1), Y = cn)$	$P(\psi_2(1), Y = cn)$	$P(\psi_3(1), Y = cn)$
Mean	0.5187715	0.5187800	0.5187855	0.5187765
Standard deviation	0.057440	0.057450	0.057445	0.057465
For k =2 (Second-harmonic)	$P(\psi_0(2), Y = cn)$	$P(\psi_1(2), Y = cn)$	$P(\psi_2(2), Y = cn)$	$P(\psi_3(2), Y = cn)$
Mean	0.7780974	0.7780899	0.7780956	0.7780959
Standard deviation	0.109391	0.109390	0.109389	0.109381
For k =3 (Third harmonic)	$P(\psi_0(3), Y = cn)$	$P(\psi_1(3), Y = cn)$	$P(\psi_2(3), Y = cn)$	$P(\psi_3(3), Y = cn)$
Mean	1.2973874	1.2973900	1.2973851	1.2973881
Standard deviation	0.234904	0.234911	0.234901	0.234909
For k =4 (Fourth harmonic)	$P(\psi_0(4), Y = cn)$	$P(\psi_1(4), Y = cn)$	$P(\psi_2(4), Y = cn)$	$P(\psi_3(4), Y = cn)$
Mean	0.1118186	0.1118190	0.1118179	0.1118188
Standard deviation	0.220256	0.220269	0.220261	0.220260
LG fault condition (cf1)				
For k=0 (d.c)	$P(\psi_0(0), Y = cf1)$	$P(\psi_1(0), Y = cf1)$	$P(\psi_2(0), Y = cf1)$	$P(\psi_3(0), Y = cf1)$
Mean	0.0037195	0.0037190	0.0037189	0.0037198
Standard deviation	0.0001148	0.0001150	0.0001149	0.0001146
For k =1 (Fundamental component)	$P(\psi_0(1), Y = cf1)$	$P(\psi_1(1), Y = cf1)$	$P(\psi_3(1), Y = cf1)$	$P(\psi_3(1), Y = cf1)$
Mean	0.0846630	0.0846632	0.0846635	0.0846629
Standard deviation	0.0093741	0.0093744	0.0093742	0.0093749
For k =2 (Second-harmonic)	$P(\psi_0(2), Y = cf1)$	$P(\psi_1(2), Y = cf1)$	$P(\psi_2(2), Y = cf1)$	$P(\psi_3(2), Y = cf1)$
Mean	0.1269850	0.1269848	0.1269844	0.1269851
Standard deviation	0.0178521	0.0178524	0.0178529	0.0178519
For k =3 (Third harmonic)	$P(\psi_0(3), Y = cf1)$	$P(\psi_1(3), Y = cf1)$	$P(\psi_2(3), Y = cf1)$	$P(\psi_3(3), Y = cf1)$
Mean	0.211732	0.2117321	0.2117328	0.2117319
Standard deviation	0.0383365	0.0383360	0.0383359	0.0383361
For k =4 (Fourth harmonic)	$P(\psi_0(4), Y = cf1)$	$P(\psi_1(4), Y = cf1)$	$P(\psi_2(4), Y = cf1)$	$P(\psi_3(4), Y = cf1)$
Mean	0.0182489	0.0182486	0.0182485	0.0182490
Standard deviation	0.0359469	0.0359468	0.0359462	0.0359460
LL fault condition (cf2)				
For k=0 (d.c)	$P(\psi_0(0), Y = cf2)$	$P(\psi_1(0), Y = cf2)$	$P(\psi_2(0), Y = cf2)$	$P(\psi_3(0), Y = cf2)$
Mean	0.0019137	0.0019135	0.0019137	0.0019137
Standard deviation	0.0000590	0.0000589	0.0000598	0.0000593
For k =1 (Fundamental component)	$P(\psi_0(1), Y = cf2)$	$P(\psi_1(1), Y = cf2)$	$P(\psi_2(1), Y = cf2)$	$P(\psi_3(1), Y = cf2)$
Mean	0.0435581	0.0435589	0.0435588	0.0435590
Standard deviation	0.0048230	0.0048233	0.0048228	0.0048231
For k =2 (Second Harmonic)	$P(\psi_0(2), Y = cf2)$	$P(\psi_1(2), Y = cf2)$	$P(\psi_2(2), Y = cf2)$	$P(\psi_3(2), Y = cf2)$
Mean	0.0653330	0.0653339	0.0653333	0.0653329

TABLE 2. *(Continued)* **Information table.**

Standard deviation	0.0091851	0.0091877	0.0091860	0.0091859
For k =3 (third harmonic)	$P(\psi_0(3), Y = cf\,2)$	$P(\psi_1(3), Y = cf\,2)$	$P(\psi_2(3), Y = cf\,2)$	$P(\psi_3(3), Y = cf\,2)$
Mean	0.1089350	0.1089351	0.1089357	0.1089356
Standard deviation	0.0197239	0.0197240	0.0197236	0.0197238
For k =4 (Fourth harmonic)	$P(\psi_0(4), Y = cf\,2)$	$P(\psi_1(4), Y = cf\,2)$	$P(\psi_2(4), Y = cf\,2)$	$P(\psi_3(4), Y = cf\,2)$
Mean	0.0093889	0.0093881	0.0093888	0.0093880
Standard deviation	0.0184940	0.0184950	0.0184945	0.0184949
LLG fault condition (cf3)				
For k=0 (d.c)	$P(\psi_0(0), Y = cf\,3)$	$P(\psi_1(0), Y = cf\,3)$	$P(\psi_2(0), Y = cf\,3)$	$P(\psi_3(0), Y = cf\,3)$
Mean	0.00131110	0.0013115	0.0013100	0.0013109
Standard deviation	0.0000404	0.0000403	0.0000410	0.0000403
For k =1 (Fundamental component)	$P(\psi_0(1), Y = cf\,3)$	$P(\psi_1(1), Y = cf\,3)$	$P(\psi_2(1), Y = cf\,3)$	$P(\psi_3(1), Y = cf\,3)$
Mean	0.0298183	0.0298182	0.0298188	0.029810
Standard deviation	0.0033019	0.0033016	0.0033019	0.0033013
For k =2 (Second-harmonic)	$P(\psi_0(2), Y = cf\,3)$	$P(\psi_1(2), Y = cf\,3)$	$P(\psi_2(2), Y = cf\,3)$	$P(\psi_3(2), Y = cf\,3)$
Mean	0.0447245	0.0447239	0.0447240	0.0447241
Standard deviation	0.0062869	0.0062870	0.0062877	0.0062879
For k =3 (Third harmonic)	$P(\psi_0(3), Y = cf\,3)$	$P(\psi_1(3), Y = cf\,3)$	$P(\psi_2(3), Y = cf\,3)$	$P(\psi_3(3), Y = cf\,3)$
Mean	0.0745729	0.0745719	0.0745721	0.0745729
Standard deviation	0.0135019	0.0135022	0.0135020	0.0135029
For k =4 (Fourth harmonic)	$P(\psi_0(4), Y = cf\,3)$	$P(\psi_1(4), Y = cf\,3)$	$P(\psi_2(4), Y = cf\,3)$	$P(\psi_3(4), Y = cf\,3)$
Mean	0.0064272	0.0064273	0.0064269	0.0064271
Standard deviation	0.0126609	0.0126606	0.0126601	0.0126610
LLL fault condition (cf4)				
For k=0 (d.c)	$P(\psi_0(0), Y = cf\,4)$	$P(\psi_1(0), Y = cf\,4)$	$P(\psi_2(0), Y = cf\,4)$	$P(\psi_3(0), Y = cf\,4)$
Mean	0.0010086	0.0010089	0.0010080	0.0010086
Standard deviation	0.0000311	0.0000310	0.0000319	0.0000312
For k =1 (Fundamental component)	$P(\psi_0(1), Y = cf\,4)$	$P(\psi_1(1), Y = cf\,4)$	$P(\psi_2(1), Y = cf\,4))$	$P(\psi_3(1), Y = cf\,4)$
Mean	0.0229581	0.0229582	0.0229589	0.0229575
Standard deviation	0.0025429	0.0025433	0.0025427	0.0025430
For k =2 (Second-harmonic)	$P(\psi_0(2), Y = cf\,4)$	$P(\psi_1(2), Y = cf\,4)$	$P(\psi_2(2), Y = cf\,4)$	$P(\psi_3(2), Y = cf\,4)$
Mean	0.0344333	0.0344344	0.0344340	0.0344341
Standard deviation	0.0048410	0.0048411	0.0048409	0.0048412
For k =3 (Third harmonic)	$P(\psi_0(3), Y = cf\,4)$	$P(\psi_1(3), Y = cf\,4)$	$P(\psi_2(3), Y = cf\,4)$	$P(\psi_3(3), Y = cf\,4)$
Mean	0.0574159	0.0574160	0.0574151	0.0574154
Standard deviation	0.0103950	0.0103957	0.0103959	0.0103955
For k =4 (Fourth harmonic)	$P(\psi_0(4), Y = cf\,4)$	$P(\psi_1(4), Y = cf\,4)$	$P(\psi_2(4), Y = cf\,4)$	$P(\psi_3(4), Y = cf\,4)$
Mean	0.0049480	0.0049487	0.0049481	0.0049489
Standard deviation	0.0097470	0.0097478	0.0097480	0.0097479

TABLE 3. GNB based prediction of fault type.

ECPA Phaselet Coefficients					Predicted Probability of					Predicted Class
$\psi_{pl}(0)$	$\psi_{pl}(1)$	$\psi_{pl}(2)$	$\psi_{pl}(3)$	$\psi_{pl}(4)$	Class 0 *(Normal condition)*	Class 1 *(LG fault)*	Class 2 *(LL Fault)*	Class 3 *(LLG Fault)*	Class 4 *(LLL Fault)*	
0.022964	0.003748	0.001928	0.00132	0.001016	**0.268547**	5.7859E-82	2.11624E-53	2.16095E-33	1.353210E-01	*Class 0*
0.02251	0.003674	0.00189	0.001294	0.000996	**0.208857**	4.1165E-82	1.83439E-53	2.05082E-33	1.347590E-01	*Class 0*
0.022826	0.003725	0.001917	0.001312	0.00101	**0.309814**	5.2201E-82	2.02674E-53	2.12704E-33	1.351510E-01	*Class 0*
0.022476	0.003668	0.001887	0.001292	0.000995	**0.18921**	4.0163E-82	1.81550E-53	2.04307E-33	1.347190E-01	*Class 0*
0.023048	0.003761	0.001935	0.001325	0.00102	**0.223437**	6.1669E-82	2.17368E-53	2.18223E-33	1.354260E-01	*Class 0*
0.582174	0.09501	0.048882	0.033463	0.025764	0.0000	**0.021640**	3.81413E-05	1.68707E-11	2.275490E-06	*Class 1*
0.464819	0.075858	0.039029	0.026717	0.02057	0.0000	**0.050141**	1.44310E-10	4.49829E-15	3.307250E-04	*Class 1*
0.466043	0.076058	0.039131	0.026788	0.020625	0.0000	**0.055376**	1.69433E-10	4.93477E-15	3.162460E-04	*Class 1*
0.460156	0.075097	0.038637	0.026449	0.020364	0.0000	**0.033688**	7.80308E-11	3.16126E-15	3.914210E-04	*Class 1*
0.581089	0.094833	0.048791	0.0334	0.025716	0.0000	**0.024000**	3.48858E-05	1.57225E-11	2.398440E-06	*Class 1*
0.832142	0.135805	0.069871	0.04783	0.036826	0.0000	2.2013E-33	**6.29876E-02**	1.07925E-05	4.971690E-13	*Class 2*
0.751286	0.122609	0.063082	0.043183	0.033248	0.0000	7.3630E-19	**9.97781E-02**	2.65564E-07	1.435200E-10	*Class 2*
0.901904	0.14719	0.075729	0.05184	0.039913	0.0000	2.2543E-49	**4.71542E-03**	1.63916E-04	2.180050E-15	*Class 2*
0.865728	0.141286	0.072691	0.049761	0.038312	0.0000	1.1080E-40	**2.33093E-02**	4.22517E-05	3.876630E-14	*Class 2*
0.87362	0.142574	0.073354	0.050215	0.038662	0.0000	1.6619E-42	**1.72300E-02**	5.73816E-05	2.092040E-14	*Class 2*
0.939028	0.153248	0.078846	0.053974	0.041556	0.0000	3.4540E-59	5.18117E-04	**5.82477E-04**	9.881820E-17	*Class 3*
0.940435	0.153478	0.078964	0.054055	0.041619	0.0000	1.4042E-59	4.71026E-04	**6.09729E-04**	8.761040E-17	*Class 3*
1.131119	0.184597	0.094975	0.065015	0.050057	0.0000	1.8395E-124	5.71194E-13	**5.60019E-02**	1.140600E-24	*Class 3*
1.140445	0.186119	0.095758	0.065551	0.05047	0.0000	3.0000E-128	1.41707E-13	**6.41977E-02**	4.262630E-25	*Class 3*
0.947265	0.154593	0.079537	0.054448	0.041921	0.0000	1.7247E-61	2.93507E-04	**7.58847E-04**	4.877790E-17	*Class 3*
0.070875	0.011567	0.005951	0.004074	0.003137	0.0000	4.3897E-67	4.82097E-47	4.92616E-31	**1.864410E-01**	*Class 4*
0.037882	0.006182	0.003181	0.002177	0.001676	0.0000	3.6012E-77	2.23516E-51	1.19763E-32	**1.533570E-01**	*Class 4*
0.000306	0.00005	0.000026	0.000018	0.000014	0.0000	1.5905E-89	1.49580E-56	1.54337E-34	**1.071010E-01**	*Class 4*
0.004134	0.000675	0.000347	0.000238	0.000183	0.0000	3.1772E-88	5.16978E-56	2.41793E-34	**1.118300E-01**	*Class 4*
0.005576	0.00091	0.000468	0.00032	0.000247	0.0000	9.7458E-88	8.23024E-56	2.86184E-34	**1.136180E-01**	*Class 4*

This module acts as a potential transformer (PT) for sensing the 3-phase transmission line voltage. The sampling rate of NI-9242 is the same as that of NI-9246 [23].

IV. NI-9467: It is a C series GPS synchronization module used to provide the necessary synchronized sampling clock pulse per second (PPS) signal to the PMU along with the location information (latitude and longitude) of the PMU [24].

V. NI-9401: It is a 5V/TTL, 8 channel, 100ns C series digital relay driver module used to generate the trip signal to open the circuit breaker for protecting the transmission line in the case of a fault. The trip signal is a 5 Volt DC which is fed to the relay module to drive the circuit breaker with a faster rate, which in turn isolates the transmission line in case of fault detection [25].

The experimental setup, cRIO-9066 along with the C series module measures three-phase voltage and current signals at the sending end of the transmission line are passed through an anti-aliasing filter with 1 kHz of the lower cut-off frequency. The three-phase current signal is transmitted to Dell Workstation for further processing. The LabVIEW software installed on the Workstation is used for analyzing and visualizing the signals using phaselet transform for perception, comprehension and prediction of the transmission line faults at a higher speed.

A. PHASELET BASED PERCEPTION AND COMPREHENSION OF THE TRANSMISSION LINE

The fault perception based on the phasor computed over one cycle of the AC signal of 50 Hz takes more than 20 ms. It is obvious that the fault perception time using FCDFT is much more than 20ms. Hence, the trip signal is issued only after 20ms [15]. In reference [12], Rajaraman reported the real-time fault analysis, which is completed within 2–3 cycles after fault inception. The perception based on the phaselet algorithm is more compared to that of FCDFT, which computes phasor for every 20 ms. Hence the fault perception time based on the phaselet algorithm is much less than that of FCDFT. Table 1 shows the fault perception time using a Phaselet algorithm for detecting the fault. Instant of fault indicates the time at which the fault has applied. Instant of detection indicates the time at which the fault was detected. The difference between the fault instant and the instant of detection gives the total time taken to detect the fault (fault perception). Table 1 shows that the detection time of the fault is on an average of 8 ms. Thus, the perception of

fault using the phaselet algorithm on the transmission line is much greater compared to that of the conventional FCDFT algorithm.

B. PREDICTION USING GAUSSIAN NAÏVE BAYES (GNB)

Gaussian Naïve Bayes (GNB) technique has been used for predicting the type of fault. A number of tests have been conducted by applying different types of fault using a fault-creating block to demonstrate the prediction capability for real-time fault. Mean and standard deviation of phaselet are estimated for each fault (i.e., normal state, LG fault, LL fault, LLG fault, and LLL fault) condition at different frequencies (d.c., fundamental, 2nd harmonic, 3rd harmonic and 4th harmonic) for model construction as shown in Table 2. For example, under no-fault condition, at k=0 (D.C. component), mean of 0.0227913 and standard deviation of 0.000703 is achieved for 1st Phaselet (ψ_0). Similarly, the mean of 0.0227500 and a standard deviation of 0.000789 is achieved for the second Phaselet (ψ_1). The information in table 2 is utilized for finding the PDF using equation (9). Table 3 represents the prediction stage by considering a new data set of phaselet coefficients derived from the three-phase current, whose fault type is to be predicted. The first five columns show the equivalent three-phase Phaselet coefficients of ECPA of the input currents at d.c., fundamental frequency, second harmonic, third harmonic and fourth harmonic. Columns six through ten presents the conditional probability of each fault, which is calculated for each attribute. The highest probability value of the corresponding fault class shown in the bold letter is considered as prediction obtained using the GNB method.

For example, consider the first row of table 3, which represents Phaselet coefficients 0.022964, 0.003748, 0.001928, 0.00132 and 0.001016 at d.c., fundamental, 2nd harmonic, 3rd harmonic and 4th harmonic respectively. The conditional probability found for each class is 0.268547, 5.7859E-82, 2.11624E-53, 2.16095E-33 and 1.353210E-01 for class0 (normal state cn), class1 (LG fault cf1), class2 (LL fault cf2), class3 (LLG fault cf3) and class 4 (LLL fault cf4) respectively. It can be observed that the highest conditional probability of 0.268547, belongs to class0 (i.e. no-fault condition). Thus, the new test data is predicted as class0 (normal state). The predicted result is compared with the actual prediction obtained by the SEL-311C transmission protection relay. It is found that the result is showing an accuracy of 100% with quick detection.

V. CONCLUSION

PMUs with their real-time phasor measurements enhance the situational awareness of the power system. This paper proposes an expeditious detection of faults on the transmission line, using Phaselets calculated from Synchronized phasor measurements from PMUs. The synchrophasor measurements from the PMUs are taken online and the Phaselets are calculated. Subsequently, the Gaussian Naïve Bayes technique has been used for predicting the type of fault, thereby enhancing situational awareness. The proposed Phaselet based expeditious detection method was implemented using LabVIEW as it is equipped with visual displays that can be used by power system operators for initiating enhanced SA based control and protection decisions. LabVIEW based virtual instrumentation has the feature of designing of SAVT for laboratory prototype implementation. The real-time analysis validates the most important requirement for speed and efficiency in restoring the defective transmission line during different faults. The future scope of the proposed work is to predict the location of the fault accurately on the transmission line and thus further leading to increased situational awareness.

REFERENCES

[1] A. G. Phadke and J. S. Thorp, *Synchronized Phasor Measurements and Their Applications*. New York, NY, USA: Springer, 2008.

[2] A. G. Phadke and T. Bi, "Phasor measurement units, WAMS, and their applications in protection and control of power systems," *J. Mod. Power Syst. Clean Energy*, vol. 6, no. 4, pp. 619–629, 2018.

[3] S. Ghosh, D. Ghosh, and D. K. Mohanta, "Situational awareness enhancement of smart grids using intelligent maintenance scheduling of phasor measurement sensors," *IEEE Sensors J.*, vol. 17, no. 23, pp. 7685–7693, Dec. 2017.

[4] S. Ghosh, D. Ghosh, and D. K. Mohanta, "Impact assessment of reliability of phasor measurement unit on situational awareness using generalized stochastic Petri nets," *Int. J. Electr. Power Energy Syst.*, vol. 93, pp. 75–83, Dec. 2017.

[5] J. Giri, M. Parashar, J. Trehern, and V. Madani, "The situation room: Control center analytics for enhanced situational awareness," *IEEE Power Energy Mag.*, vol. 10, no. 5, pp. 24–39, Sep./Oct. 2012.

[6] E. Ghahremani and I. Kamwa, "Dynamic state estimation in power system by applying the extended Kalman filter with unknown inputs to phasor measurements," *IEEE Trans. Power Syst.*, vol. 26, no. 4, pp. 2556–2566, Nov. 2011.

[7] I. Kamwa, S. R. Samantaray, and G. Joós, "On the accuracy versus transparency trade-off of data-mining models for fast-response PMU-based catastrophe predictors," *IEEE Trans. Smart Grid*, vol. 3, no. 1, pp. 152–161, Mar. 2012.

[8] P. Gopakumar, M. J. B. Reddy, and D. K. Mohanta, "Adaptive fault identification and classification methodology for smart power grids using synchronous phasor angle measurements," *IET Gener., Transmiss. Distrib.*, vol. 9, no. 2, pp. 133–145, Jan. 2015.

[9] P. Gopakumar, M. J. B. Reddy, and D. K. Mohanta, "Transmission line fault detection and localisation methodology using PMU measurements," *IET Gener., Transmiss. Distrib.*, vol. 9, no. 11, pp. 1033–1042, Aug. 2015.

[10] K. R. Dhenuvakonda, A. R. Singh, M. P. Thakre, B. S. Umre, A. Kumar, and R. C. Bansal, "Effect of SSSC-based SSR controller on the performance of distance relay and adaptive approach using synchronized measurement," *Int. Trans. Elect. Energy Syst.*, vol. 28, no. 11, p. e2620, 2018.

[11] A. A. Majd, H. Samet, and T. Ghanbari, "k-NN based fault detection and classification methods for power transmission systems," *Protection Control Mod. Power Syst.*, vol. 2, no. 1, p. 32, 2017.

[12] P. Rajaraman, N. A. Sundaravaradan, B. Mallikarjuna, M. J. B. Reddy, and D. K. Mohanta, "Robust fault analysis in transmission lines using synchrophasor measurements," *Protection Control Mod. Power Syst.*, vol. 3, no. 1, p. 14, 2018.

[13] P. Gopakumar, B. Mallikajuna, M. J. B. Reddy, and D. K. Mohanta, "Remote monitoring system for real time detection and classification of transmission line faults in a power grid using PMU measurements," *Protection Control Mod. Power Syst.*, vol. 3, no. 1, p. 16, 2018.

[14] B. Kumar, A. Yadav, and A. Y. Abdelaziz, "Synchrophasors assisted protection scheme for the shunt-compensated transmission line," *IET Gener., Transmiss. Distrib.*, vol. 11, no. 13, pp. 3406–3416, Sep. 2017.

[15] B. Huang and T. Nengling, "Phaselet algorithm based differential protection for large generator," *Przegląd Elektrotechniczny*, vol. 89, no. 1a, pp. 243–247, 2013.

[16] X. Jin, R. Gokaraju, R. Wierckx, and O. Nayak, "High speed digital distance relaying scheme using FPGA and IEC 61850," *IEEE Trans. Smart Grid*, vol. 9, no. 5, pp. 4383–4393, Sep. 2018.
[17] S. S. Y. Ng, Y. Xing, and K. L. Tsui, "A naive Bayes model for robust remaining useful life prediction of lithium-ion battery," *Appl. Energy*, vol. 118, pp. 114–123, Apr. 2014.
[18] D. K. Babu, Y. Ramadevi, and K. V. Ramana, "RGNBC: Rough Gaussian Naïve Bayes classifier for data stream classification with recurring concept drift," *Arabian J. Sci. Eng.*, vol. 42, no. 2, pp. 705–714, 2017.
[19] P. Dangeti, *Statistics for Machine Learning*. Birmingham, U.K.: Packt, Jul. 2017.
[20] P. Kundur, *Power System Stability and Control*. New Delhi, India: McGraw-Hill, 2012.
[21] *Datasheet NI 9203*. Accessed: May 23, 2019. [Online]. Available: https://www.ni.com/en-in/support/model.crio-9066.html
[22] *Datasheet NI 9246*. Accessed: May 23, 2019. [Online]. Available: http://www.ni.com/pdf/manuals/376372a.pdf
[23] *Datasheet NI 9242*. Accessed: May 23, 2019. [Online]. Available: http://www.ni.com/pdf/manuals/376130b_02.pdf
[24] *Datasheet NI-9467 C Series Synchronization Module*. Accessed: May 23, 2019. [Online]. Available: http://www.ni.com/pdf/manuals/373230c.pdf
[25] *Datasheet NI 9401*. Accessed: May 23, 2019. [Online]. Available: http://www.ni.com/pdf/manuals/374068a_02.pdf

KUNJA BIHARI SWAIN received the B.Tech. degree in electronics and instrumentation engineering from the National Institute of Science and Technology, Berhampur, India, in 2008, and the M.E. degree in instrumentation and control from the Birla Institute of Technology, Ranchi, India, in 2014. He is currently pursuing the Ph.D. degree with the Centurion University of Technology and Management, Odisha, India. His current research interests include wide area situational awareness and power systems.

SATYA SOPAN MAHATO received the Ph.D. degree in electronics and communication engineering from Jadavpur University, India. He is currently an Associate Professor with the National Institute of Science and Technology, Odisha, India. He has authored or coauthored several scientific articles in international journals. His research interests include T-CAD, microelectronics, solar cells, reliability physics, and characterization of advanced CMOS and novel devices.

MURTHY CHERUKURI (M'13) received the B.Tech. degree in electrical and electronics engineering from Jawaharlal Nehru Technological University, Kakinada, India, in 2007, and the M.E. degree in power systems and the Ph.D. Engg. degree from the Birla Institute of Technology, Ranchi, India, in 2010 and 2015, respectively. He is currently a Professor with the Department of Electrical and Electronics Engineering, National Institute of Science and Technology, Berhampur, India. His current research interests include power system reliability, wide area measurement systems, and phasor measurement unit placement. He was a recipient of the POSOCO Power System Award, in 2016.